Journal of
Electronic Imaging

JElectronicImaging.org

Improved opponent color local binary patterns: an effective local image descriptor for color texture classification

Francesco Bianconi
Raquel Bello-Cerezo
Paolo Napoletano

SPIE. IS&T imaging.org

Francesco Bianconi, Raquel Bello-Cerezo, Paolo Napoletano, "Improved opponent color local binary patterns: an effective local image descriptor for color texture classification," *J. Electron. Imaging* **27**(1), 011002 (2017), doi: 10.1117/1.JEI.27.1.011002.

Journal of Electronic Imaging 27(1), 011002 (Jan/Feb 2018)

Improved opponent color local binary patterns: an effective local image descriptor for color texture classification

Francesco Bianconi,[a,*] **Raquel Bello-Cerezo,**[a] **and Paolo Napoletano**[b]
[a]Università degli Studi di Perugia, Department of Engineering, Perugia, Italy
[b]Università degli Studi di Milano-Bicocca, Department of Informatics, Systems and Communication, Milano, Italy

Abstract. Texture classification plays a major role in many computer vision applications. Local binary patterns (LBP) encoding schemes have largely been proven to be very effective for this task. Improved LBP (ILBP) are conceptually simple, easy to implement, and highly effective LBP variants based on a point-to-average thresholding scheme instead of a point-to-point one. We propose the use of this encoding scheme for extracting intra- and interchannel features for color texture classification. We experimentally evaluated the resulting improved opponent color LBP alone and in concatenation with the ILBP of the local color contrast map on a set of image classification tasks over 9 datasets of generic color textures and 11 datasets of biomedical textures. The proposed approach outperformed other grayscale and color LBP variants in nearly all the datasets considered and proved competitive even against image features from last generation convolutional neural networks, particularly for the classification of biomedical images. *© 2017 SPIE and IS&T* [DOI: 10.1117/1.JEI.27.1.011002]

Keywords: local binary patterns; image classification; color texture; convolutional neural networks.

Paper 170495SS received Jun. 17, 2017; accepted for publication Sep. 6, 2017; published online Dec. 5, 2017.

1 Introduction

Texture is one of the fundamental visual properties of objects, materials, and scenes. Understanding texture is, therefore, essential in a wide range of applications, such as surface inspection and grading, content-based image retrieval, object recognition, material classification, remote sensing, and medical image analysis. As a consequence, research on texture has been attracting significant attention for at least 40 years, and a large number of visual descriptors are now available in the literature—for an overview, we refer the reader to Refs. 1 and 2.

During the last two decades, the "bag of features" (BoF) paradigm has emerged as one of the most effective approaches to texture analysis.[3–5] This scheme is best explained by resorting to a parallel with the "bag of words" model, whereby a text is represented by the statistical, orderless distribution of its words over a predefined dictionary. Likewise, the BoF represents images by the distribution of local patterns regardless of their spatial distribution.[6] One possible implementation of the BoF model is represented by a class of methods known as histogram of equivalent patterns (HEP).[7] Descriptors of this class sample the input images densely and assign each local image patch to one visual word among those in the dictionary. The image representation is the probability distribution (histogram) of the visual words over the dictionary. In the HEP, the mapping image patch → visual word is typically a function (usually referred to as the "kernel function") of the gray levels of pixels in the patch. In this approach, the dictionary is defined *a priori* and coincides with the codomain of the kernel function. Local binary patterns (LBPs) and related methods are all instances of this general scheme.[6,7]

Extensions of this strategy to the color domain involve comparing the color (or multispectral) pixel values instead of the gray levels.[8] This area, however, has received significantly less attention than the grayscale counterpart. One of the first extensions of LBP to color images was the opponent color LBP (OCLBP),[9] in which, as we detail in Sec. 3, the LBP operator is applied to each color channel separately as well as to pairs of color channels. Herein, we propose a conceptually simple yet effective improvement on this method. We denote our descriptor as improved opponent color LBP (IOCLBP) and show, experimentally, that it can significantly outperform OCLBP in color texture classification.

In the remainder of the paper, we first provide some background in Sec. 2 and then introduce IOCLBP in Sec. 3. We discuss the experimental activity in Sec. 4 and summarize the results in Sec. 5. Some final considerations and directions for future studies conclude the paper (Sec. 6).

2 Background

Few would object that LBP is one the most prominent and widely investigated texture descriptors ever. The method first appeared with this name in 1996[10] and was popularized in a later work,[11] which has now become a classic. Together, the two papers have so far received no fewer than 9500 citations (Source: Scopus; visited on August 17, 2017). Keys to the success of this method are the ease of implementation, low computational demand, and high discrimination accuracy. A lot of LBP variations also exist; so many, indeed, that in a recent review Liu et al.[12] correctly stated that their number is so large that it is becoming more and more difficult—even to the expert in the field—to grasp them all. In comparison, color variants have received significantly less attention in the literature.

The problem of integrating texture and color information into combined descriptors has attracted the interest of

*Address all correspondence to: Francesco Bianconi, E-mail: bianco@ieee.org

researchers since early on.[13] The existing approaches can be categorized in different ways, as for instance described in Refs. 13–17 but in synthesis there are three main classes:

- pure color methods (or spectral methods),
- pure texture methods, and
- hybrid methods.

Spectral methods describe the color content of the image regardless of its spatial distribution. By contrast, pure texture methods—also referred to as "intensity texture features"[15]—are based on the spatial variation of luminance (gray level) but discard chrominance. These are the standard texture descriptors, such as LBP, Gabor filters, wavelets, etc. Finally, hybrid methods combine color and texture information together. The approaches belonging to the last group can be further classified into "parallel," "sequential," and "integrative."[18]

In parallel approaches, color and textures are computed separately and then combined together through late or early fusion, as for instance in LBP and color percentiles,[19] LBP and color information features,[20] and LBP and color histogram.[21]

Sequential approaches usually involve some preprocessing to convert the input image to single channel (for instance through color quantization), after that the resulting image can be processed through a grayscale descriptor. Examples are the sequential classifier described by Bianconi et al.[22] and the multilayer scheme proposed by Lumini et al.[23]

Integrative approaches are possibly the most common strategy for extending LBP to the color domain. They consist of applying the LBP operator to each color channel separately[24–26] and/or to pairs of channels jointly.[27,9] Color and spatial data can also be combined in a vectorial way, as for instance in local color vector binary patterns,[28] local angular patterns,[29] color intensity local mapped pattern,[30] and 3-D LBPs.[31] Another strategy consists of defining a suitable total ordering in the color space and uses this as a replacement for the natural gray-level ordering. This class of methods has been recently investigated extensively by Ledoux et al.[32] Possible implementations of this scheme involve defining a suitable notion of distance and a reference point in the color space chosen, as proposed in Refs. 33 and 34.

As we detail in Sec. 3, IOCLBP considers intra- and interchannel features[35]—just as OCLBP—but with a different local thresholding scheme. While in OCLBP, the peripheral pixels are thresholded at the value of the central pixel, thresholding in IOCLBP is based on the average value. In the grayscale domain, the same approach has been used to define improved LBPs (ILBP),[36] which generally works better than LBP,[37] but as far as we know this idea has not been extended to the color domain. The method proposed here can be, therefore, considered as an extension of ILBP to color textures.

3 Improved Opponent Color Local Binary Patterns

Let us consider a local image neighborhood $\mathcal{N} = \{\mathbf{x}_0, \mathbf{x}_1, \dots, \mathbf{x}_n\}$ composed of a central point $\mathbf{x}_0$ and n peripheral points $\mathbf{x}_i$, $i \in \{1, \dots, n\}$. For the sake of simplicity, we shall assume the neighborhood be center-symmetric with the peripheral points arranged circularly around the central one (Fig. 1), though this restriction is not essential.[38] Let also a pattern $\mathcal{P}$ be defined as an instance of $\mathcal{N}$, i.e., $\mathcal{P} = \{\mathbf{p}_0, \mathbf{p}_i, \dots, \mathbf{p}_n\}$, where $\mathbf{p}_i$ denotes a generic property of $\mathbf{x}_i$, such as the gray-level intensity, color triplet, or multispectral data. (In the remainder, we indicate such property in boldface when is a vector and in normal font when is a scalar.)

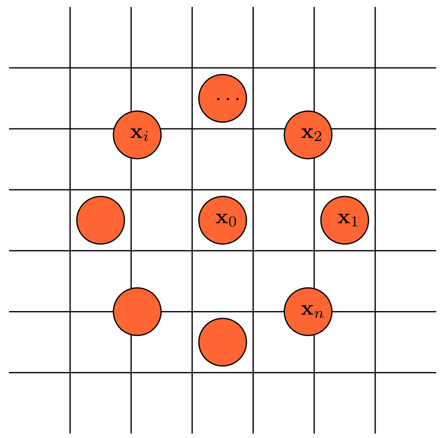

Fig. 1 A center-symmetric neighborhood.

In LBP, a pattern $\mathcal{P}$ is assigned a unique decimal code (or, equivalently, a visual word) in the following way:

$$f_{\mathrm{LBP}}(\mathcal{P}) = \sum_{i=1}^{n} 2^{i-1}\phi(g_0, g_i), \tag{1}$$

where

$$\phi(x, y) = \begin{cases} 0 & \text{if } x \le y \\ 1 & \text{otherwise} \end{cases}, \tag{2}$$

and g_i in this case is the gray level of $\mathbf{x}_i$. Image features are the dense, orderless statistical distribution over the set of possible codes.

Mäenpää and Pietikäinen[9] proposed an extension of this scheme to the color domain by considering intra- and interchannel features. Intrachannel features are obtained just by computing LBP on each color channel, whereas for a pair of channels (u, v) the interchannel features are defined as follows:

$$f_{\mathrm{OCLBP}_{u,v}}(\mathcal{P}) = \sum_{i=1}^{n} 2^{i-1}\phi(p_{0,u}, p_{i,v}), \tag{3}$$

where $p_{i,v}$ indicates the intensity of the i'th pixel in the v'th channel. For a color space with C channels, there are in principle $K = 2 \times C!/[2!(C-2)!]$ ways through which interchannel features can be computed. However, to avoid redundancy and reduce the overall number of features, for a pair of channels (u, v) it is customary to retain only one of the two possible permutations—either (u, v) or (v, u).[14,9] The number of interchannel pairs, therefore, reduces to $K = C!/[2!(C-2)!]$.

IOCLBP differs from OCLBP in that both intra- and interchannel features are computed using a point-to-average scheme instead of a point-to-point one. In formulas, we have

$$f_{\mathrm{IOCLBP}_{u,v}}(\mathcal{P}) = \sum_{i=0}^{n} 2^{i}\phi(\bar{p}_u, p_{i,v}), \tag{4}$$

Method	Acronym	Reference	Year	No. of features
LBP variants				
Texture spectrum ●●●	TS	He and Wang[31]	1990	2502
Local binary patterns ●●●	LBP	Ojala et al.[59]	2002	108
Improved local binary patt. ●●●	ILBP	Jin et al.[34]	2004	213
Opponent color local binary patt. ●●●	OCLBP	Mäenpää and Pietikäinen[52]	2005	648
OCLBP + local color contrast ●●●	OCLBP + LCC	This paper	2017	1416
Completed local binary patterns ●●●	CLBP	Guo et al.[29]	2010	324
oRGB local binary patterns ●●●	oRGB-LBP	Banerji et al.[6]	2011	324
Local color vector local binary patt. ●●●	LCVBP	Lee et al.[42]	2012	432
Extended local binary patterns ●●●	ELBP	Liu et al.[46]	2012	321
Lbp + local color contrast ●●●	LBP + LCC	Cusano et al.[20]	2014	876
Improved opp. color local bin. patt. ●●●	IOCLBP	This paper	2017	1287
IOCLBP + local color contrast ●●●	IOCLBP + LCC	This paper	2017	1500
Hybrid colour local binary patterns ●●●		Fekriershad and Tajeripour[24]	2017	432
CNN based features				
Caffe-Alex fully connected ●●●	Caffe-Alex-FC	Krizhevsky et al.[39]	2012	4096
VGG-M fully connected ●●●	VGG-M-FC	Chatfield et al.[18]	2016	4096
VGG-VeryDeep-16 fully connected ●●●	VGG-VD-16-FC	Simonyan and Zisserman[69]	2015	4096
VGG-VeryDeep-19 fully connected ●●●	VGG-VD-19-FC		2015	4096
ResNet-50 fully connected ●●●	ResNet-50-FC	He et al.[32]	2016	2048

Key to symbols: ●●● = color descriptor; ●●● = greyscale descriptor

Fig. 2 Summary list of the methods included in the experiments.

where

$$\bar{p}_u = \frac{1}{n+1}\sum_{i=0}^{n} p_{i,u}. \tag{5}$$

It is easy to see from Eqs. (1) and (3) that the number of directional features generated by LBP and OCLBP is 2^{n-1} and $(C+K)\times 2^{n-1}$, respectively, whereas in IOCLBP, we have $C\times(2^n-1)$ intrachannel features (the "zero" pattern is by definition impossible, hence the -1 in the formula) and $K\times 2^n$ interchannel features. Variations of LBP, such as the rotation invariant ($\mathrm{LBP}^{\mathrm{ri}}$) and the uniform, rotation-invariant version ($\mathrm{LBP}^{\mathrm{riu2}}$) apply seamlessly to IOCLBP as well. The number of features in this case (see Fig. 2) can be computed through invariant theory.

Let us just recall here that "necklaces" are strings of λ characters over an alphabet of size σ, being equivalent those necklaces that can be transformed into one another through a discrete rotation. It can be shown that the number of intrinsically different necklaces is

$$\mathcal{K}(\lambda,\sigma) = \frac{1}{\lambda}\sum_{v|\lambda}\phi\left(\frac{\lambda}{v}\right)\sigma^{v}, \tag{6}$$

where $\phi()$ indicates Euler's totient function and v the divisor of λ (see Ref. 39, Sec. 13.3 for details). Clearly, rotation-invariant LBPs ($\mathrm{LBP}^{\mathrm{ri}}$) are a particular case of necklaces with $\lambda = n$ and $\sigma = 1$; therefore, their number can be easily computed though Eq. (6). The interested reader will find further considerations on this and a table with precomputed values in Ref. 40.

3.1 *Color Spaces*

IOCLBP can in principle be defined over any color space, provided that all the channels have the same range of values. In our experiments, we considered the RGB, Ohta's (Ref. 41, Sec. 4.5), and opponent color spaces (Ref. 41, Sec. 4.4). In the last two cases, suitable normalization factors were applied to guarantee that the range of each channel was the [0, 1] interval. In the remainder, we shall use subscripts "oht" and "opp" to denote the results obtained with these color spaces and no subscripts for the RGB space or grayscale images.

3.2 *Concatenation of IOCLBP and Local Color Contrast Features*

We also propose the use of IOCLBP in combination with local color contrast (LCC).[42] LCC is a descriptor designed to be robust with respect to changes in illumination. It preserves a useful part of color information and, at the same time, discards the part that is often affected by changes in illumination. Let us just recall, here, that LCC is based on the angle θ, in the color space, between the color of the central pixel and the average color of the peripheral pixels, i.e.,

$$\theta = \begin{cases} 0 & : \|\mathbf{p}_0\|\cdot\|\bar{\mathbf{p}}\| = 0 \\ \arccos\left(\frac{\langle \mathbf{p}_0, \bar{\mathbf{p}}\rangle}{\|\mathbf{p}_0\|\cdot\|\bar{\mathbf{p}}\|}\right) & : \text{otherwise} \end{cases}, \tag{7}$$

where $\bar{\mathbf{p}}_0$, here, stands for the color of the central point and $\bar{\mathbf{p}}$ for the average color of the peripheral points. Symbols $\langle\cdot,\cdot\rangle$ and $\|\cdot\|$ indicate inner product and Euclidean norm, respectively.

We computed LCC features by applying the ILBP operator on the angle map resulting from transforming the input image through Eq. (7)

$$f_{\mathrm{LCC}}(\mathcal{P}) = \sum_{i=0}^{n} 2^i \phi(\bar{\theta}, \theta_0), \tag{8}$$

where

ID	Name	No. of classes	No. of samples per class	Sample images
1	KTH-TIPS	10	81	
2	KTH-TIPS2b	11	432	
3	Outex-00013	68	20	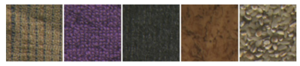
4	Outex-00014	68	60	
5	PlanLeaves	20	60	
6	RawFooT	68	184	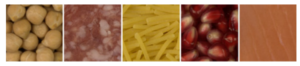
7	STex	476	16	
8	USPTex	191	12	
9	V×C TSG	42	12	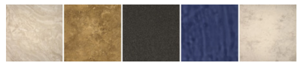

Fig. 3 Generic color textures: summary table.

ID	Name	No. of classes	No. of samples per class	Sample images
1	BioMediTechRPE	4	Variable	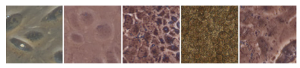
2	BreakHis 40×	2	Variable	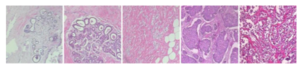
3	BreakHis 100×	2	Variable	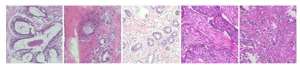
4	BreakHis 200×	2	Variable	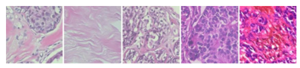
5	BreakHis 400×	2	Variable	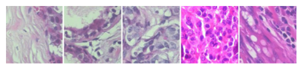
6	Epistroma	2	Variable	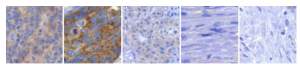
7	Kather	8	625	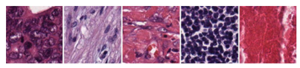
8	LiverAge	4	Variable	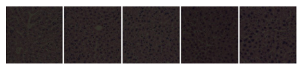
9	LiverGender-AL	2	Variable	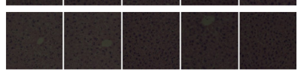
10	LiverGender-CR	2	Variable	
11	Lymphoma	3	Variable	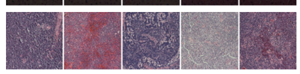

Fig. 4 Biomedical textures: summary table.

$$\bar{\theta} = \frac{1}{n+1}\sum_{i=0}^{n}\theta_i. \tag{9}$$

We finally combined IOCLBP and LCC by concatenating the respective feature vectors. Based on the results of previous experiments,[42] we applied a scaling factor of $w = 0.25$ to LCC. We maintained this setting with the akin methods used for comparison, i.e., LBP + LCC and OCLBP + LCC.

4 Experiments

To evaluate the effectiveness of IOCLBP and IOCLBP + LCC, we carried out a set of image classification experiments using 20 datasets of color texture images as described in Sec. 4.1. For comparison, we considered 10 LBPs variants and 5 image descriptors based on pretrained convolutional neural networks (Sec. 4.2). Classifier and accuracy evaluation procedure are detailed in Sec. 4.3.

4.1 *Datasets*

We considered 9 datasets of generic color texture images representing materials and scenes (Sec. 4.1.1, Fig. 3) and 11 datasets of biomedical images (Sec. 4.1.2, Fig. 4).

4.1.1 *Generic color textures*

KTH-TIPS: Ten classes representing materials such as aluminum foil, bread, corduroy, cotton, cracker, linen, orange peel, sandpaper, sponge, and styrofoam.[43,44] One sample of each class was acquired at 9 different scales, 3 poses, and under 3 illumination conditions, resulting in 81 images per class. The dimension of the images is 200 px $\times$ 200 px.

KTH-TIPS2b: An extension of KTH-TIPS containing one more class, four samples for each class instead of one, and one additional illumination condition. The whole dataset contains 432 images for each class.[45,44] The image dimension is the same as in KTH-TIPS.

Outex-00013: Sixty-eight texture classes from Outex's test suite TC-00013.[46] They represent heterogeneous materials, such as barley, cardboard, fabric, natural stone, paper, sandpaper, and wool. For each class, there are 20 image samples of dimension 128 px $\times$ 128 px, which have no variation in scale, rotation angle, or illumination conditions.

Outex-00014: The same classes as in Outex-00013; however, in this case, each sample was acquired under three different lighting sources: a 2300-K horizon sunlight, a 2856-K incandescent CIE A, and a 4000-K fluorescent TL84 lamp, respectively. As a result, there are 60 samples for each class instead of 20. The image dimension is the same as in Outex-00014. For both Outex-00013 and Outex-00014, it is important to point out that to maintain a uniform evaluation protocol (see Sec. 4.3) for all the datasets considered here, we used different subdivisions into train and test set than those provided with the TC-00013 and TC-00014 test suites.

PlantLeaves: Images of leaves from 20 different species of plants acquired under controlled imaging conditions through a planar scanner.[47] There are 60 samples for each class, each of dimension 128 px $\times$ 128 px.

RawFooT: Sixty-eight classes representing different types of raw food, such as grain, fish, fruit, meat, pasta, and vegetables.[1,48,49] Each sample was acquired under 46 different lighting conditions that differ in the direction of light, color, and/or the illumination intensity. Other viewing conditions as scale and rotation angle are invariable. We subdivided each image into four nonoverlapping images of dimension 400 px $\times$ 400 px and this way obtained $46 \times 4 = 184$ image samples for each class.

STex: Four hundred seventy-six color texture images representing objects, materials and scenes, such as bark, buildings, flowers, leather, metal, stones, tiles, and wood. The pictures have been acquired "in the wild" around in the city of Salzburg, Austria.[50] The dataset comes in two different resolutions—i.e., 1024 px $\times$ 1024 px and 512 px $\times$ 512 px—of which we used the second one in our experiments. We subdivided the original images into 16 nonoverlapping samples of dimension 128 px $\times$ 128 px.

USPTex: One hundred ninety-one classes of color textures with 12 samples per class.[51,52] The classes represent materials such as seeds, rice, and fabric but also road scenes, vegetation, walls, clouds, and soil. The images have been acquired in the wild and have a dimension of 128 px $\times$ 128 px.

V $\times$ C TSG: Forty-two classes of ceramic tiles acquired under controlled and steady imaging conditions in the V $\times$ C laboratory at the Polytechnic University of Valencia, Valencia, Spain.[53,54] There are 14 base classes, each identified by its commercial denomination—e.g., Agata, Berlin, Firenze, Lima, Oslo, and Venice, and each class comes in three subclasses (grades), which are very similar and difficult to differentiate even to the trained eye. The original images have different resolution and can be either rectangular or square, and the number of samples varies from class to class. Herein, we retained 12 samples for each class and cropped each image to a central square window of dimension $\min(W, H) \times \min(W, H)$, where W and H are the width and height of the original image, respectively.

4.1.2 *Biomedical textures*

BioMediTechRPE: Image samples of pluripotent stem cell-derived retinal pigment epithelium (RPE) cells—the layer of the eye between the neurosensory retina and the choroid.[55,56] The dataset includes three classes representing different stages of RPE maturation indicated as fusiform, epithelioid, and cobblestone, respectively, plus a fourth class sharing features common to two or more of the other classes. The number of samples per class varies from 150 to 949. Of each image sample we retained a central region of dimension 480 px $\times$ 480 px.

BreakHis: Histological images of breast tumour tissue from 82 patients collected at the P&D Laboratory—Pathological Anatomy and Cytopathology, Parana, Brazil.[57,58] The images have been acquired using four different magnification factors, i.e., 40×, 100×, 200×, and 400×, and in our experiments, we considered each group as a dataset on its own, which in the remainder we indicate as BreakHis 40×, BreakHis 100×, etc. The images are labeled into two main classes ("benign" and "malignant" lesions) and four subclasses each, i.e., adenosis, fibroadenoma, Phyllodes tumor, and tubular adenoma (benign lesions) and carcinoma, lobular carcinoma, mucinous carcinoma, and papillary carcinoma (malignant lesions), respectively. In the experiments, we only considered the two-class subdivision into benign and malignant lesions. The original images have dimension 700 px $\times$ 460 px, which we centrally cropped to a square of 460 px $\times$ 460 px.

Epistroma: Histological images of colorectal cancer from 643 patients enrolled at Helsinki University Central Hospital, Helsinki, Finland, from 1989 to 1998.[59,60] The tissue samples have been stained with diaminobenzidine and hematoxylin and labeled into two classes: epithelium (825 samples) and stroma (551 samples). The dimension of the images varies from 172 px $\times$ 172 px to 2372 px $\times$ 2372 px.

Kather: Histological images of colorectal cancer from 10 patients enrolled at the University Medical Center Mannheim, Mannheim, Germany.[61–63] The tissue samples have been stained with hematoxylin and eosin (H&E), digitally scanned, and labeled into eight classes: epithelium, simple stroma, complex stroma, immune cells, debris, normal mucosa glands,

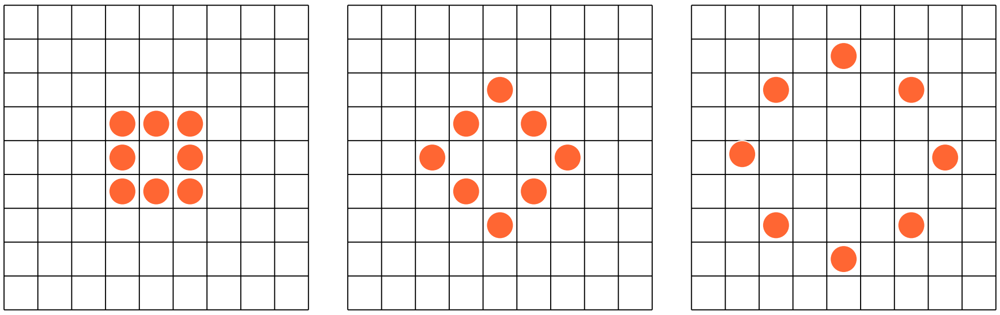

Fig. 5 Pixel neighborhoods corresponding to resolutions 1, 2, and 3.

adipose tissue, and background. For each class, there is a total of 625 image samples of dimension 150 px × 150 px.

LiverAge: Histological images representing liver tissue from a total of 30 female mice on an unrestricted diet.[64,65] The samples are classified into four classes depending on the age of the subject, i.e., 1, 6, 16, and 24 month, respectively. The tissue specimens have been H&E stained by a single operator to avoid interobserver variability. The original images have a dimension of 1388 px × 1040 px of which we retained a central crop of size 1040 px × 1040 px.

LiverGender AL: A dataset analogous to LiverAge with samples representing liver tissue from six-month-old male and female mice on an *ad-libitum* diet.[64,65] The classification is two-way in this case: male and female subjects. The other settings are the same as in the LiverAge dataset.

LiverGender CR: Similar to LiverGender AL, but in this case, the samples come from six-month-old male and female mice on a caloric restriction diet.[64,65] The classification is again between male and female subjects, while the other settings are the same as in LiverAge and LiverGender AL.

Lymphoma: A collection of samples from malignant lymphoma biopsies sectioned and stained with H&E.[66] The dataset comprises three classes representing different types of the disorder: lymphocytic leukemia, follicular lymphoma, and mantle cell lymphoma. The samples have been prepared by different pathologists at different sites and, as a consequence, show a large degree of staining variation. The original images have a dimension of 1388 px × 1040 px, which again we cropped to a central portion of size 1040 px × 1040 px.

4.2 *Comparison with Other Methods*

We comparatively evaluated the effectiveness of IOCLBP with that of 10 LBP variants and 5 pretrained CNNs as detailed as follows (see also Fig. 2 for a round-up).

4.2.1 *Local binary patterns variants*

We considered the following LBP variants (sorted by publication date):

- texture spectrum,[67]
- LBP,[11]
- ILBP,[36]
- OCLBP,[9]
- completed LBP,[68]
- oRGB-LBP,[24]
- extended LBP,[69]
- local color vector binary patterns,[28]
- combination of LBPs and LCC,[42] and
- hybrid color LBP.[25]

For each of the aforementioned methods, a rotation-invariant, multiresolution feature vector was obtained by concatenating the rotation-invariant feature vectors computed at resolution 1, 2, and 3 (Fig. 5). Rotation invariance was obtained by grouping together all the local patterns that can be transformed into one another by a discrete rotation, which is usually referred to as the "ri" configuration—see also Refs. 11 and 40 on this point. The number of features generated by each descriptor is shown in Fig. 2. For details about each of the aforementioned methods, we refer the reader to the given references.

4.2.2 *Pretrained convolutional neural networks*

For calibration purposes, we also included five feature vectors from pretrained convolutional neural networks, specifically, Caffe-AlexNet, VGG-M, VGG-VeryDeep-16, VGG-VeryDeep-19, and ResNet-50 as, respectively, described in Refs. 70–73 For each pretrained model, we considered as features the L_2-normalized output the last fully connected layer. This approach, which is usually referred to as the "FC" configuration, proved the most effective in recent comparative studies.[74]

4.3 *Classification and Accuracy Evaluation*

Classification was based on the parameter-free nearest-neighbor classifier with L_1 ("cityblock") distance. Accuracy estimation was performed through split-sample validation with stratified sampling, i.e., half of the samples of each class were used to train the classifier and the remaining half to test it. The estimated accuracy was the fraction of samples of the test set that were classified correctly. For a stable estimation, the results (Tables 1 and 2) were averaged over 100 random splits into train and test set.

5 Results and Discussion

5.1 *Accuracy*

Table 1 summarizes the average classification accuracy obtained with the generic color textures. As can be seen, IOCLBP + LCC and IOCLBP emerged as the best methods among the LBP variants in eight datasets out of nine. Comparison with CNN-based features shows that ResNet-50-FC outperformed the other descriptors in six dataset out of nine, while IOCLBP achieved the best accuracy in the remaining three.

Table 1 Generic color textures: overall accuracy by descriptor and dataset.

	Dataset ID (see Fig. 3)								
Descriptor	1	2	3	4	5	6	7	8	9
				LBP variants					
CLBP	95.8	95.9	81.2	83.5	74.5	94.9	82.0	88.0	88.0
ELBP	93.8	94.7	83.3	86.5	78.7	96.1	78.3	84.2	91.7
HCLBP	95.6	96.5	86.8	86.7	79.8	97.4	86.8	91.4	90.5
ILBP	95.4	95.1	85.5	88.6	76.9	97.1	80.4	87.0	90.5
IOCLBP	96.2	98.5	*91.0*	*91.9*	77.7	97.7	91.5	92.7	94.9
$\text{IOCLBP}_{\text{oht}}$	93.6	96.6	87.5	86.5	72.5	97.3	85.3	89.0	92.3
$\text{IOCLBP}_{\text{opp}}$	94.4	97.2	88.0	87.8	80.0	97.1	82.4	87.3	95.7
IOCLBP + LCC	96.8	**98.8**	90.0	91.2	78.8	97.4	**93.6**	**95.2**	*96.0*
LBP	94.2	93.5	80.9	83.7	73.8	95.2	74.2	82.1	89.4
LBP + LCC	94.9	95.9	83.6	85.1	79.3	96.7	83.1	89.7	93.7
LCVBP	96.3	97.6	82.8	83.5	75.4	97.3	90.0	93.6	91.5
OCLBP	95.2	97.8	90.9	91.5	76.9	97.0	88.6	90.3	93.3
$\text{OCLBP}_{\text{oht}}$	92.7	95.4	85.4	84.7	72.3	96.8	82.2	85.3	90.9
$\text{OCLBP}_{\text{opp}}$	92.8	96.1	86.0	86.2	80.7	96.6	78.2	82.2	93.5
OCLBP + LCC	96.5	98.5	89.9	90.8	77.9	96.8	91.7	93.4	94.9
oRGB-LBP	**97.3**	97.9	84.8	86.3	**84.1**	97.0	89.7	**93.7**	92.6
TS	92.9	94.6	81.3	83.9	76.2	96.6	78.7	85.3	91.2
				CNN-based features					
Caffe-Alex-FC	98.7	99.0	82.9	83.8	71.6	97.6	91.2	95.7	80.0
VGG-M-FC	98.7	99.3	84.9	83.3	74.0	98.4	94.4	97.6	79.2
VGG-VD-16-FC	99.4	99.5	84.3	83.5	77.4	98.6	94.3	96.8	79.5
VGG-VD-19-FC	99.4	99.4	83.8	82.8	78.0	98.6	94.1	96.6	74.6
ResNet-50-FC	*99.6*	*99.7*	87.2	86.0	*86.6*	*98.9*	*97.4*	*99.2*	83.2

Note: Datasets IDs: 1, KTH-TIPS; 2, KTH-TIPS2b; 3, Outex-13; 4, Outex-14; 5, PlantLeaves; 6, RawFooT; 7, STex; 8, USPTex; and 9, V × C TSG.
Note: For each dataset, boldface figures indicate the highest value among the hand-designed descriptors and italic values indicate the highest among all descriptors.

With the biomedical textures (Table 2), the scenario was decidedly more favorable to LBP variants, which proved superior to CNN-based features in 8 dataset out of 11. In particular, IOCLBP + LCC emerged as the absolute best-performing methods in 6 datasets out of 11.

Interestingly, the superiority of CNN-based methods with generic color textures, and, by contrast, that of LBP variants—distinguishably the descriptors proposed in this paper—with biomedical textures seems consistent with recent findings[75] suggesting that CNNs are more suitable when there is high intraclass variability, whereas LBP works better with homogeneous, fine-grained textures with low intraclass variability.

Finally, no clear trend emerged as for the best color space among the ones considered (i.e., RGB, Ohta, and opponent space), with the results showing a rather dataset-dependent trend.

Table 2 Biomedical textures: overall accuracy by descriptor and dataset.

	Dataset ID (see Fig. 4)										
Descriptor	1	2	3	4	5	6	7	8	9	10	11
					LBP variants						
CLBP	83.2	81.6	78.5	77.2	74.7	**97.1**	86.1	82.6	85.8	93.6	73.6
ELBP	83.7	80.6	75.7	74.7	71.0	92.4	78.1	88.5	90.3	96.3	66.1
HCLBP	84.2	82.5	80.3	78.1	75.6	93.3	87.8	90.5	94.2	97.8	72.3
ILBP	83.7	81.1	80.2	76.9	73.0	92.6	82.2	86.3	92.1	95.7	69.3
IOCLBP	85.4	93.1	92.2	92.7	91.0	91.8	92.2	97.0	95.7	98.6	86.0
$\text{IOCLBP}_{\text{oht}}$	85.0	92.6	*93.5*	92.9	90.8	93.2	92.0	96.7	96.9	98.0	79.6
$\text{IOCLBP}_{\text{opp}}$	84.3	91.5	91.2	90.0	87.4	93.0	91.2	96.5	96.0	98.4	81.4
IOCLBP + LCC	85.3	*93.7*	92.9	*93.8*	*91.9*	92.8	*93.4*	*97.9*	*97.8*	98.6	*89.5*
LBP	83.9	78.3	74.6	72.8	69.9	92.3	75.4	83.9	89.4	94.7	66.0
LBP + LCC	84.7	83.1	78.9	79.6	75.7	93.2	84.0	88.9	96.1	98.6	74.8
LCVBP	85.4	89.8	87.9	87.0	86.1	91.8	90.9	96.4	95.7	**98.7**	77.4
OCLBP	85.2	91.5	91.2	92.1	90.5	91.8	91.0	96.8	95.3	98.6	82.4
$\text{OCLBP}_{\text{oht}}$	85.1	91.7	92.5	92.6	90.4	93.2	91.6	95.8	95.5	97.9	79.0
$\text{OCLBP}_{\text{opp}}$	84.2	90.4	90.4	89.4	87.5	93.2	90.4	95.6	95.3	**98.7**	79.7
OCLBP + LCC	**85.4**	92.4	92.4	93.2	91.5	92.3	92.5	97.5	97.6	98.6	87.8
oRGB-LBP	85.0	86.7	85.2	84.9	84.4	93.1	85.0	94.3	95.2	98.6	73.5
TS	84.0	80.8	78.0	76.4	72.7	92.0	80.0	86.1	90.3	94.9	68.0
					CNN-based features						
Caffe-Alex-FC	86.8	85.2	83.8	84.9	84.9	94.3	83.3	81.6	95.8	*99.5*	73.8
VGG-M-FC	86.8	89.5	87.0	88.6	83.7	95.1	85.1	85.1	95.5	98.1	75.6
VGG-VD-16-FC	86.3	89.7	87.0	87.0	83.4	95.3	86.0	74.2	91.0	92.6	71.1
VGG-VD-19-FC	86.5	88.8	86.4	85.6	83.4	94.5	84.1	73.2	82.0	93.5	63.6
ResNet-50-FC	*87.5*	93.4	90.9	91.6	89.8	*97.3*	89.6	87.3	90.5	97.4	77.1

Note: Datasets IDs: 1, BioMediTechRPE; 2, BreakHis40×; 3, BreakHis100×; 4, BreakHis200×; 5, BreakHis400×; 6, Epistroma; 7, Kather; 8, LiverAgeing; 9, LiverGender-AL; 10, LiverGender-CR; and 11, Lymphoma.
Note: For each dataset, boldface figures indicate the highest value among the hand-designed descriptors and italic values indicate the highest among all descriptors.

5.2 *Computational Demand*

Table 3 shows, for each descriptor, the average feature extraction (FE) time per image, the average classification (CL) time per problem, and the group (Q_{FE} and Q_{CL}) into which the population is divided by the corresponding quartiles. The results show that the proposed approaches entail a higher workload than other LBP variants, as one would reasonably expect. Compared with CNN-based features, IOCLBP and IOCLBP + LCC emerge as slower in the feature extraction step but faster in the classification step due to the lower-dimensional feature vectors. The table also shows that there are no significant differences in the computational demand depending on the color space used.

Table 3 Computational demand: FE = average feature extraction time per image, CL = average classification time per problem; Q_{FE} and Q_{CL} are the corresponding groups (I = fastest group and IV = slowest group). Values are averaged over all the datasets.

Descriptor	FE (s)	Q_{FE}	CL (s)	Q_{CL}
	LBP variants			
CLBP	0.773	II	0.298	I
ELBP	1.145	III	0.295	I
HCLBP	1.749	III	3.624	IV
ILBP	0.423	I	0.197	I
IOCLBP	2.207	IV	1.279	III
IOCLBP + LCC	3.202	IV	2.056	III
LBP	0.338	I	0.118	I
LBP + LCC	1.227	III	1.043	II
LCVBP	3.005	IV	0.403	II
OCLBP	1.644	III	0.620	II
OCLBP+LCC	2.636	IV	1.403	III
oRGB-LBP	1.895	III	0.300	II
TS	0.781	II	2.615	III
	CNN-based features			
Caffe-Alex-FC	0.089	I	3.844	IV
VGG-M-FC	0.162	I	3.849	IV
VGG-VD-16-FC	0.375	I	3.874	IV
VGG-VD-19-FC	0.470	II	3.846	IV
ResNet-50-FC	0.727	II	1.917	III

6 Conclusions

In this work, we have introduced a conceptually simple, easy-to-implement yet highly discriminative local descriptor for color images, which we have called IOCLBP. Experimentally, we have demonstrated the superiority of either IOCLBP alone and/or in combination with LCC with respect to akin methods (LBP variants) for the classification of color texture images. In our experiments, IOCLBP's accuracy was comparable to that of features based on pretrained convolutional networks—and even better in most cases—but with the advantage of IOCLBP being conceptually much easier to implement and training free. Remarkably, the proposed descriptor proved particularly suitable for the classification of fine-grained color textures, as, for instance, those contained in histological images.

Acknowledgments

This work was partially supported by the Department of Engineering, the Università degli Studi di Perugia, Italy, under project BioMeTron—Fundamental research Grant D.D. 20/2015 and by the Spanish Government under Project No. AGL2014-56017-R.

References

1. C. Cusano, P. Napoletano, and R. Schettini, "Evaluating color texture descriptors under large variations of controlled lighting conditions," *J. Opt. Soc. Am. A* **33**(1), 17–30 (2016).
2. X. Xie and M. Mirmehdi, "A galaxy of texture features," in *Handbook of Texture Analysis*, M. Mirmehdi, X. Xie, and J. Suri, Eds., pp. 375–406, Imperial College Press, London (2008).
3. M. Crosier and L. Griffin, "Texture classification with a dictionary of basic image features," in *Proc. of the 26th IEEE Conf. on Computer Vision and Pattern Recognition*, Anchorage (2008).
4. S. Kondra and V. Torre, "Texture classification using three circular filters," in *Proc. of the 6th Indian Conf. on Computer Vision, Graphics and Image Processing*, Bhubaneswar, India, pp. 429–434 (2008).
5. J. Zhang et al., "Local features and kernels for classification of texture and object categories: a comprehensive study," *Int. J. Comput. Vision* **73**(2), 213–238 (2007).
6. F. Bianconi and A. Fernández, "A unifying framework for LBP and related methods," *Stud. Comput. Intell.* **506**, 17–46 (2014).
7. A. Fernández, M. X. Álvarez, and F. Bianconi, "Texture description through histograms of equivalent patterns," *J. Math. Imaging Vision* **45**(1), 76–102 (2013).
8. M. Pietikäinen et al., *Local Binary Patterns for Still Images*, Springer, London (2011).
9. T. Mäenpää and M. Pietikäinen, "Texture analysis with local binary patterns," in *Handbook of Pattern Recognition and Computer Vision*, 3rd ed., C. H. Chen and P. S. P. Wang, Eds., pp. 197–216, World Scientific Publishing, Singapore (2005).
10. T. Ojala, M. Pietikäinen, and D. Harwood, "A comparative study of texture measures with classification based on feature distributions," *Pattern Recognit.* **29**(1), 51–59 (1996).
11. T. Ojala, M. Pietikäinen, and T. Mäenpää, "Multiresolution gray-scale and rotation invariant texture classification with local binary patterns," *IEEE Trans. Pattern Anal. Mach. Intell.* **24**(7), 971–987 (2002).
12. L. Liu et al., "Local binary features for texture classification: taxonomy and experimental study," *Pattern Recognit.* **62**, 135–160 (2017).
13. D. Ilea and P. Whelan, "Image segmentation based on the integration of colour–texture descriptors—a review," *Pattern Recognit.* **44**(10–11), 2479–2501 (2011).
14. F. Bianconi et al., "Theoretical and experimental comparison of different approaches for color texture classification," *J. Electron. Imaging* **20**(4), 043006 (2011).
15. E. Cernadas et al., "Influence of normalization and color space to color texture classification," *Pattern Recognit.* **61**, 120–138 (2017).
16. E. González et al., "Automatic characterization of the visual appearance of industrial materials through colour and texture analysis: an overview of methods and applications," *Adv. Opt. Technol.* **2013**, 503541 (2013).
17. F. Khan et al., "Compact color-texture description for texture classification," *Pattern Recognit. Lett.* **51**, 16–22 (2015).
18. C. Palm, "Color texture classification by integrative co-occurrence matrices," *Pattern Recognit.* **37**(5), 965–976 (2004).
19. M. Niskanen, O. Silvén, and H. Kauppinen, "Color and texture based wood inspection with non-supervised clustering," in *Proc. of the 12th Scandinavian Conf. on Image Analysis (SCIA 2001)*, Bergen, Norway, pp. 336–342 (2001).
20. P. Liu et al., "Fusion of color histogram and LBP-based features for texture image retrieval and classification," *Inf. Sci.* **390**, 95–111 (2017).
21. L. Serpa-Andrade et al., "A proposal based on color descriptors and local binary patterns histogram as support tool in presumptive diagnosis of hiatus hernia," in *Proc. of the IEEE Int. Autumn Meeting on Power, Electronics and Computing (ROPEC 2014)*, Ixtapa, Mexico (2014).
22. F. Bianconi et al., "Texture classification through combination of sequential colour texture classifiers," *Lect. Notes Comput. Sci.* **4756**, 231–240 (2007).
23. A. Lumini, L. Nanni, and S. Brahnam, "Multilayer descriptors for medical image classification," *Comput. Biol. Med.* **72**, 239–247 (2016).
24. S. Banerji, A. Verma, and C. Liu, "Novel color LBP descriptors for scene and image texture classification," in *Proc. of the 2011 Int. Conf. on Image Processing, Computer Vision, and Pattern Recognition*, Las Vegas, Vol. 2, pp. 537–543 (2011).
25. S. Fekriershad and F. Tajeripour, "Color texture classification based on proposed impulse-noise resistant color local binary patterns and significant points selection algorithm," *Sens. Rev.* **37**(1), 33–42 (2017).
26. O. Losson and L. Macaire, "CFA local binary patterns for fast illuminant-invariant color texture classification," *J. Real Time Image Process.* **10**(2), 387–401 (2015).
27. T. Mäenpää and M. Pietikäinen, "Classification with color and texture: jointly or separately?" *Pattern Recognit.* **37**(8), 1629–1640 (2004).
28. S. Lee et al., "Local color vector binary patterns from multichannel face images for face recognition," *IEEE Trans. Image Process.* **21**(4), 2347–2353 (2012).

29. C. Cusano, P. Napoletano, and R. Schettini, "Local angular patterns for color texture classification," *Lect. Notes Comput. Sci.* **9281**, 111–118 (2015).
30. T. Negri et al., "A robust descriptor for color texture classification under varying illumination," in *Proc. of the 12th Int. Joint Conf. on Computer Vision, Imaging and Computer Graphics Theory and Applications (VISAPP)*, Porto, Portugal, pp. 378–388 (2017).
31. S. Banerji, A. Sinha, and C. Liu, "New image descriptors based on color, texture, shape, and wavelets for object and scene image classification," *Neurocomputing* **117**, 173–185 (2013).
32. A. Ledoux, O. Losson, and L. Macaire, "Color local binary patterns: compact descriptors for texture classification," *J. Electron. Imaging* **25**(6), 061404 (2016).
33. G. Lian, "Rotation invariant color texture classification using multiple sub-DLBPs," *J. Visual Commun. Image Represent.* **31**, 1–13 (2015).
34. A. Porebski, N. Vandenbroucke, and L. Macaire, "Haralick feature extraction from LBP images for color texture classification," in *Proc. of the 1st Int. Workshops on Image Processing Theory, Tools and Applications*, Sousse, Tunisia (2008).
35. F. Bianconi et al., "Improved opponent colour local binary patterns for colour texture classification," *Lect. Notes Comput. Sci.* **10213**, 272–281 (2017).
36. H. Jin et al., "Face detection using improved LBP under Bayesian framework," in *Proc. of the 3rd Int. Conf. on Image and Graphics*, Hong Kong, China, pp. 306–309 (2004).
37. A. Fernández et al., "Evaluation of robustness against rotation of LBP, CCR and ILBP features in granite texture classification," *Mach. Vision Appl.* **22**(6), 913–926 (2011).
38. L. Nanni, A. Lumini, and S. Brahnam, "Local binary patterns variants as texture descriptors for medical image analysis," *Artif. Intell. Med.* **49**(2), 117–125 (2010).
39. C. Charalambides, *Enumerative Combinatorics*, Discrete Mathematics and Its Applications, Chapman and Hall/CRC Press, Boca Raton, Florida (2002).
40. E. González, F. Bianconi, and A. Fernández, "An investigation on the use of local multi-resolution patterns for image classification," *Inf. Sci.* **361**–**362**, 1–13 (2016).
41. H. Palus, "Representations of colour images in different colour spaces," in *The Colour Image Processing Handbook*, S. J. Sangwine and R.E.N. Horne, Eds., pp. 67–90, Springer, Boston, Massachusetts (1998).
42. C. Cusano, P. Napoletano, and R. Schettini, "Combining local binary patterns and local color contrast for texture classification under varying illumination," *J. Opt. Soc. Am. A* **31**(7), 1453–1461 (2014).
43. E. Hayman et al., "On the significance of real-world conditions for material classification," *Lect. Notes Comput. Sci.* **3024**, 253–266 (2004).
44. "The KTH-TIPS and KTH-TIPS2 image databases," 2004, http://www.nada.kth.se/cvap/databases/kth-tips/ (16 March 2016).
45. B. Caputo, E. Hayman, and P. Mallikarjuna, "Class-specific material categorization," in *Proc. of the IEEE Int. Conf. on Computer Vision*, Beijing, China, Vol. 2, pp. 1597–1604 (2005).
46. T. Ojala et al., "Outex—new framework for empirical evaluation of texture analysis algorithms," in *Proc. of the 16th Int. Conf. on Pattern Recognition (ICPR'02)*, Vol. 1, pp. 701–706, IEEE Computer Society, Quebec, Canada (2002).
47. D. Casanova, J. J. de Mesquita Sá, Jr., and O. Martinez Bruno, "Plant leaf identification using Gabor wavelets," *Int. J. Imaging Syst. Technol.* **19**(3), 236–243 (2009).
48. P. Napoletano, "Hand-crafted vs learned descriptors for color texture classification," *Lect. Notes Comput. Sci.* **10213**, 259–271 (2017).
49. "Rawfoot db: raw food texture database," 2015, http:projects.ivl.disco.unimib.it/rawfoot/ (28 December 2015).
50. "Salzburg texture image database (STex)," http://wavelab.at/sources/STex/ (24 May 2017).
51. A. Backes, D. Casanova, and O. Bruno, "Color texture analysis based on fractal descriptors," *Pattern Recognit.* **45**(5), 1984–1992 (2012).
52. "USPTex dataset," 2012, http://fractal.ifsc.usp.br/dataset/USPtex.php (6 January 2016).
53. F. López et al., "Performance evaluation of soft color texture descriptors for surface grading using experimental design and logistic regression," *Pattern Recognit.* **41**(5), 1744–1755 (2008).
54. "VxC TSG image database for surface grading," 2005, http://miron.disca.upv.es/vision/vxctsg (4 July 2014).
55. "BioMediTech RPE dataset," 2016, https://figshare.com/articles/BioMediTech_RPE_dataset/2070109 (16 May 2017).
56. L. Nanni et al., "Texture descriptors ensembles enable image-based classification of maturation of human stem cell-derived retinal pigmented epithelium," *PLoS One* **11**(2), e0149399 (2016).
57. "Breast cancer histopathological database (BreakHis)," 2015, http://web.inf.ufpr.br/vri/breast-cancer-database (16 May 2017).
58. F. Spanhol et al., "Breast cancer histopathological image classification using convolutional neural networks," in *Int. Joint Conf. on Neural Networks (IJCNN 2016)*, Vancouver, Canada (2016).
59. Webmicroscope, "EGFR colon TMA stroma LBP classification," 2012, http://fimm.webmicroscope.net/Research/Supplements/epistroma (16 May 2017).
60. N. Linder et al., "Identification of tumor epithelium and stroma in tissue microarrays using texture analysis," *Diagn. Pathol.* **7**(22), 1–11 (2012).
61. "Collection of texture in colorectal cancer histology," 2016, https://zenodo.org/record/53169.WRsdEPmGN0w (16 May 2017).
62. J. N. Kather et al., "Continuous representation of tumor microvessel density and detection of angiogenic hotspots in histological whole-slide images," *Oncotarget* **6**(22), 19163–19176 (2015).
63. J. N. Kather et al., "Multi-class texture analysis in colorectal cancer histology," *Sci. Rep.* **6**, 27988 (2016).
64. National Institute on Aging, "Liver age," 2008, https://ome.grc.nia.nih.gov/iicbu2008/agemap/index.html (26 May 2017).
65. L. Shamir et al., "IICBU 2008: a proposed benchmark suite for biological image analysis," *Med. Biol. Eng. Comput.* **46**(9), 943–947 (2008).
66. "Lymphoma dataset," https://ome.grc.nia.nih.gov/iicbu2008/lymphoma/index.html (16 May 2017).
67. D. C. He and L. Wang, "Texture unit, texture spectrum, and texture analysis," *IEEE Trans. Geosci. Remote Sens.* **28**(4), 509–512 (1990).
68. Z. Guo, L. Zhang, and D. Zhang, "A completed modeling of local binary pattern operator for texture classification," *IEEE Trans. Image Process.* **19**(6), 1657–1663 (2010).
69. L. Liu et al., "Extended local binary patterns for texture classification," *IEEE Trans. Image Process.* **30**(2), 86–99 (2012).
70. K. Chatfield et al., "Return of the devil in the details: delving deep into convolutional nets," in *Proc. of the British Machine Vision Conf. 2014*, Nottingham, United Kingdom (2014).
71. K. He et al., "Deep residual learning for image recognition," in *Proc. of the IEEE Computer Society Conf. on Computer Vision and Pattern Recognition*, Las Vegas, pp. 770–778 (2016).
72. A. Krizhevsky, I. Sutskever, and G. Hinton, "ImageNet classification with deep convolutional neural networks," in *Proc. of Advances in Neural Information Processing Systems*, Lake Tahoe, Vol. 2, pp. 1097–1105 (2012).
73. K. Simonyan and A. Zisserman, "A very deep convolutional networks for large-scale image recognition," in *Proc. of the 3rd Int. Conf. on Learning Representations*, San Diego (2015).
74. C. Cusano, P. Napoletano, and R. Schettini, "Combining multiple features for color texture classification," *J. Electron. Imaging* **25**(6), 061410 (2016).
75. R. Bello-Cerezo et al., "Hand-designed local image descriptors vs. off-the-shelf CNN-based features for texture classification: an experimental comparison," in *Intelligent Interactive Multimedia Systems and Services (KES-IIMSS 2017)*, Vilamoura, Portugal, Smart Innovation, Systems and Technologies, G. De Pietro et al., Eds., Vol. 76 (2017).

Francesco Bianconi received his MEng degree from the University of Perugia, Italy, and his PhD in computer-aided design from a consortium of Italian universities. He has been a visiting researcher at the University of Vigo, Spain, the University of East Anglia, UK, and Queen Mary University of London, UK. He is currently a senior lecturer in the Department of Engineering, the University of Perugia, where he conducts research on computer vision, image processing, and pattern recognition with special focus on texture and color analysis. He is an IEEE senior member.

Raquel Bello-Cerezo received her MEng degree in industrial engineering from the University of Vigo, Spain, and is currently a PhD candidate of industrial and information engineering at the University of Perugia, Italy. Her research interests are in image processing with specific focus on industrial and biomedical applications.

Paolo Napoletano received his MSc degree in telecommunications engineering from the University of Naples Federico II, Italy, and his PhD in information engineering from the University of Salerno, Italy. He is currently a postdoctoral fellow in the Department of Informatics, Systems and Communication, the University of Milan-Bicocca, Italy. He conducts research on image and video analysis, information retrieval, and pervasive healthcare.